UNIVERSITY OF COPENHAGEN
FACULTY OF SCIENCE

Ultra stable laser sources based on molecular acetylene

Author
Parisah Akrami

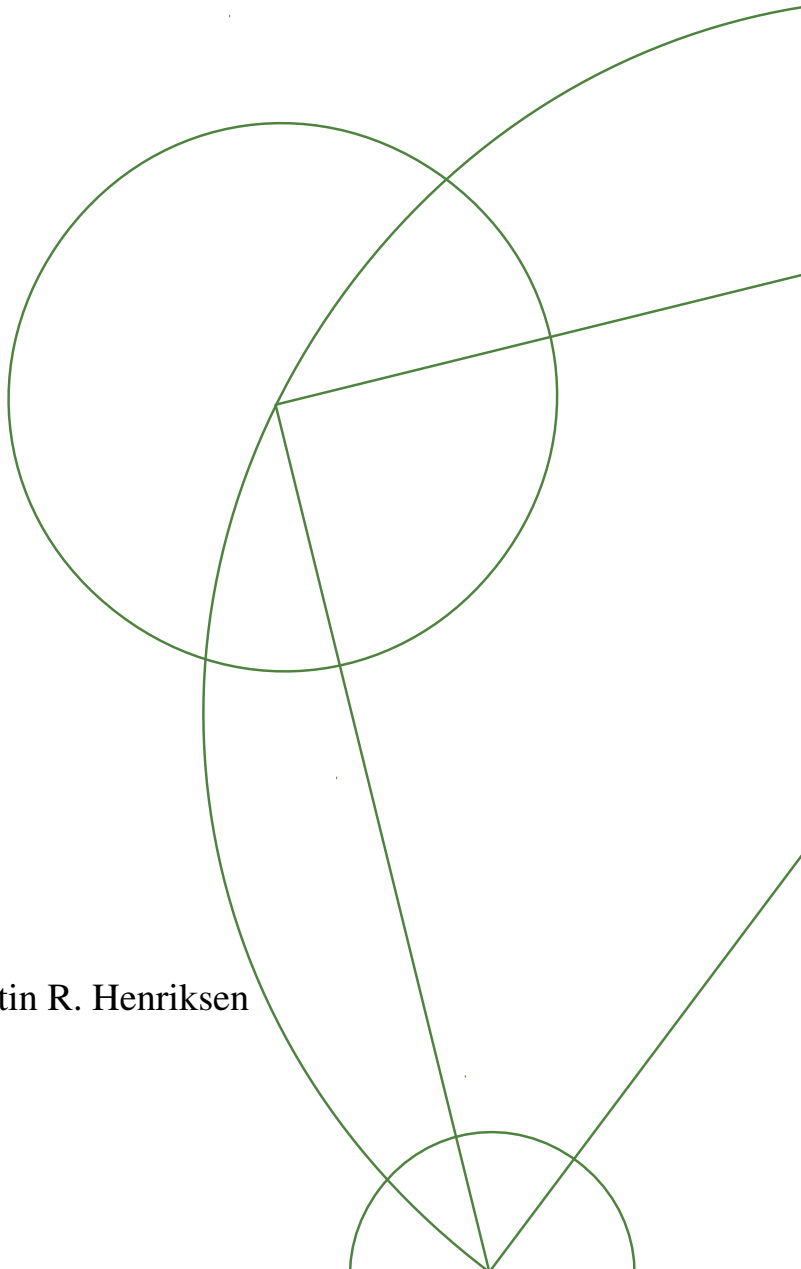

Niels Bohr Institute
Supervisor: Jan W. Thomsen and Martin R. Henriksen
Submitted: January 18, 2017

Contents

Abstract

In this thesis we present an experimental setup to perform saturated absorption spectroscopy on molecular acetylene $^{13}C_2H_2$. The hyperfine ro-vibrational transition P(16): $\nu_1+\nu_3$ at 1542.3837 nm is of interest as a frequency reference. The acetylene molecule is placed with an optical cavity for an increased interaction length. The linewidth obtained from saturation absorption spectroscopy is measured with respect to the optical cavity power. The optical cavity is locked to the frequency of the laser by use of the so-called Pound-Drever-Hall technique. This enables phase sensitive detection of the molecular transition with high signal-to-noise ratio (SNR). The saturated absorption spectroscopy revealed a linewidth which was measured to be in the megahertz regime. The pressure of the acetylene cell was larger than predicted. A relative stability of $2.22 \cdot 10^{-10}$ in a integration time of 10 seconds was measured.

1 Introduction

If we want to measure a quantity with the highest degree of accuracy, it would certainly be the frequency. It is possible today to measure frequencies better than 1 part in 10^{15}. Accurate time and frequency measurements are very important today in our society including fields such as the global trade, traffic and most sub-fields of technology and science [1]. But any measurement is done by comparison with something else. A frequency standard, also known as a frequency reference, is a well defined frequency that works as a measure for other frequencies to be calibrated against. The frequency is measured by using a common unit Hertz.

A frequency standard can actually be used as a clock having a well known stable frequency from an oscillating system, but the frequency has to be stable in a given time. This means that it must not vary in time and place. The development of more accurate clocks, showing an improvement over the last decades, from mechanical pendulum clocks, quartz clocks, atomic clocks and to optical clocks. In 1967 the second was defined as 9.192.631.770 oscillations of the transition between the two hyperfine levels of the ground state of the caesium-133 isotope. Since then any new quantum mechanical clock capable of measuring another time standard must be compared to the existing time standard [1].

Accurate clocks and time precision is of interest in modern technology, such as high speed telecommunications, stable micro wave resonators and so on. Optical clocks are great as frequency standard due to the fundamental transition frequency of a given atom or molecule. Optical clocks are currently the best candidates as frequency standards due to optical frequencies in the range of $10^{12} - 10^{15}$ Hz (THz regime). A higher frequency increases the quality factor Q which is given by ratio of the frequency of the reference oscillator and the experimentally obtainable linewidth of the reference oscillator. The relative uncertainty is proportional to the Q-factor. The plotted uncertainty for different types of clocks over the years. Optical clocks have a much lower relative uncertainty compared to other different types of clocks, see figure 1.

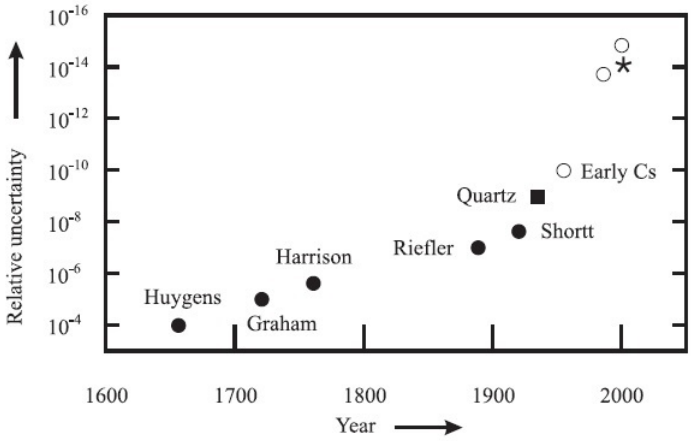

Figure 1: Figure from [1]. The relative uncertainty of different clocks over the past years. Mechanical pendulum clock (full circles); quartz clocks (full square); Cs atomic clocks (open circles); optical clocks (asterisk). The improvement of technology and experimental methods can be seen especially for optical clocks.

But constructing an optical clock requires not only accuracy. It is important to note the difference between the terms accuracy and stability. Accuracy is defined as how far a given measurement is from the ”true value”. Stability is defined as changes of a given measurement over time. By increasing the quality factor Q one can increase the stability. One can expect further improvements by the use of optical frequency standards. As long as the definition of unit is based on the hyperfine transition in caesium, these standard will serve as secondary frequency standards. They will allow more accurate

frequency ratios and eventually lead to a new definition of time.

1.1 This project

In this project we propose an experimental setup and make use of saturated absorption spectroscopy on molecular acetylene $^{13}C_2H_2$. The hyperfine ro-vibrational transition P(16): $\nu_1+\nu_3$ at 1542.3837 nm is of interest as a frequency reference. The International Bureau of Weights and Measures (BIPM) has adopted the transition of interest as a secondary frequency reference. [2]. In the setup the acetylene cell is placed within an optical cavity for an increased interaction length. The linewidth of the small dip also known as the "Lamb dip", obtained from the saturated absorption spectroscopy is measured with respect to the optical cavity power. To make sure that we have a standing wave in the cavity at all times, the cavity length is locked to the frequency of the laser by use of a so-called Pound-Drever-Hall technique. This enables phase sensitive detection of the molecular transitions with high signal-to-noise ratio.

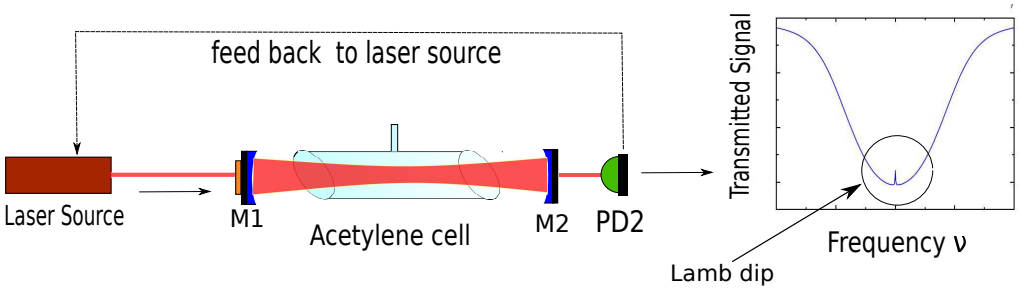

Figure 2: An optical cavity for saturated absorption spectroscopy of an absorbing molecular sample. Saturated absorption spectroscopy is obtained by the transmitted signal from the cavity. A feed back is sent back to the laser source. In our case the acetylene cell is placed within the cavity.

In the next section we will discuss briefly the interaction of light with molecules and their extra degrees of freedom which exist because of vibrations and rotations. We will be going through the acetylene absorption cell used in this setup as a frequency reference and the specific transition of interest. The different broadening mechanisms that affects our collected data will be discussed. The experimental work and different techniques used including the so-called Pound-Drever-Hall and NICE-OHMS technique, are demonstrated in section 4. Collected data from saturated absorption spectroscopy is presented. The collected data are measured, and the different results obtained are discussed in section 5. Finally a conclusion on the measured results and an outlook for future improvements.

2 Interaction of molecules and atoms with light

The whole foundation of optical frequency standards are the light-matter interaction. We need to know what happens when light interacts with matter which consists of molecules or atoms. In this section we will focus on molecules. Molecules are more complex in structure compared to atoms because they are build up by several atoms and the possibility of rotations and vibrations gives them extra degree of freedom with associated energy levels.

2.1 Energy states of molecules

Molecules are build up by more than one atom and therefore they can rotate and vibrate. Molecules have vibrational and rotational energy levels. Both of them can be combined to such that the molecule is vibrating and rotating at the same time. The energies associated with the molecular vibrations and rotations are quantized and only certain energy levels are allowed [3].

If we look at a simple diatomic molecule like C_2 or H_2, there is a binding force holding the two atoms together. This can be interpreted as the atoms being held together by a spring force with a spring constant k. The potential energy can be expressed as,

$$V(x) = \frac{1}{2}k(x - x_0)^2 \tag{1}$$

where k is the spring constant and x is the distance between two atoms and x_0 is the equilibrium.

The quantum mechanical energy spectrum for a harmonic oscillator is spaced evenly between the levels and the spacing is $\hbar\omega$, where,

$$E_n = \hbar\omega\left(n + \frac{1}{2}\right), n = 0, 1, 2, 3, ... \tag{2}$$

here $\omega = \sqrt{k/m}$.

Real diatomic molecules have vibrational energy levels that are more or less An-harmonic, thus the quantum mechanical energy spectrum is different and does not satisfy equation 2. The potential describing the binding force between the two atoms can be expressed by a so-called Morse potential. See figure 3 (a). The vibrational energy levels may be written as,

$$E_\upsilon = \hbar\omega_e\left[\left(\nu + \frac{1}{2}\right) - x_e\left(\nu + \frac{1}{2}\right)^2 + y_e\left(\nu + \frac{1}{2}\right)^3 + ...\right] \tag{3}$$

where $\nu = 0, 1, 2, 3, ...$, is the vibrational quantum number and ω_e,x_e and y_e are the anharmonicity coefficients. The ω_e represent the vibrational wavenumber with units cm^{-1}.

A diatomic molecule can also rotate, though the energy scale associated with rotations is significantly smaller. The rotations can be described as one dumbbell with two masses m_1 and m_2 held together by a massless rigid rod of length x_0, rotating about its center of mass. The moment of inertia is given by,

$$I = mx_0^2 \tag{4}$$

where m is the reduced mass and x_0 is the distance between the two masses. If the angular velocity of rotation is ω_R the angular momentum will just be $L = I\omega_R$. The kinetic energy will in this case be,

$$E = \frac{1}{2}I\omega_R^2 = \frac{L^2}{2I} \tag{5}$$

the operator L^2 has the eigenvalues $\hbar^2 L(L+1)$ known from quantum mechanics. The rotational energy for a diatomic molecule has the allowed values,

$$E_J = \frac{\hbar^2}{2I}J(J + 1) = hcBJ(J + 1), J = 0, 1, 2, ... \tag{6}$$

where B is the rotational constant and J is the rotational quantum number.

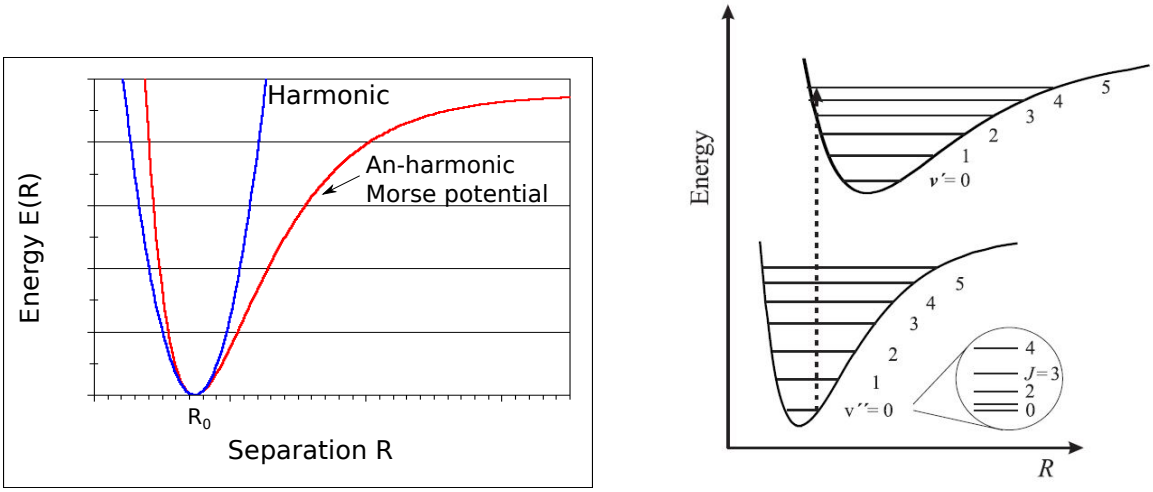

Figure 3: (a): The potential energy function as a function of the separation of the two atoms, R. R_0 is the equilibrium distance. We see that near R_0 the Morse potential resembles the harmonic potential and for larger R the an-harmonicity becomes more profound (b): The an-harmonic potential for the electronic energy level for the ground state is the bottom one and for the excited state the one above. The vibrational energy levels are noted as a ladder with the vibrational quantum number v. Each vibrational energy is split into rotational energy levels described with the quantum number J. Figure from [1].

When the diatomic molecule rotates the centrifugal force will increase the separation between the two atomic nuclei and the moment of inertia will increase too. The spacing between the rotational energy levels gets larger as J increases. The level spacing between each vibrational level decreases when ν increases compared to the harmonic oscillator with even spacing. A change in vibrational quantum number v is often accompanied by a change in rotational quantum number J. This means that rotation and vibration is coupled and so we talk about ro-vibrational transitions.

The an-harmonic Morse potential can be seen in figure 3 (b) as a function of the separation R. The electronic energy level for the ground state is the bottom one and for the excited state the one above. The vibrational energy levels are noted as a ladder with the vibrational quantum number ν. Each of the vibrational energy level is split into a series of bound rotational energy levels described by the rotational quantum number J.

In general the total energy of the molecule will be a combination of the electric (E_e), vibrational (E_ν) and rotational energies (E_J),

$$E_{tot} = E_e(R) + E_\nu + E_J = V(R) + \hbar\omega_e(\nu + \frac{1}{2}) + hcBJ(J+1) \tag{7}$$

where $V(R)$ is the electronic potential. Transitions between vibrational levels lie in the infrared region and transitions between rotational levels lie in the microwave region [3].

In our case the molecule of interest is not as simple as for a single diatomic molecule. The molecule of interest in this project is the acetylene molecule C_2H_2 where we have a strong triple bond between the C atoms and weak single bond between the C atom and the H atom, the binding force between the atoms results in vibrations, see figure 4 (a).

The acetylene molecule can vibrate in different modes compared to a simple diatomic molecule. The different vibrational modes for the acetylene molecule C_2H_2 can be seen in figure 4 (b). The arrows between each bond on each atom shows which way the atom is vibrating with respect to its position. The vibrational mode, e.g., ν_3 is for the stretching from the C-H bond. Each vibrational mode corresponds to certain transition frequencies.

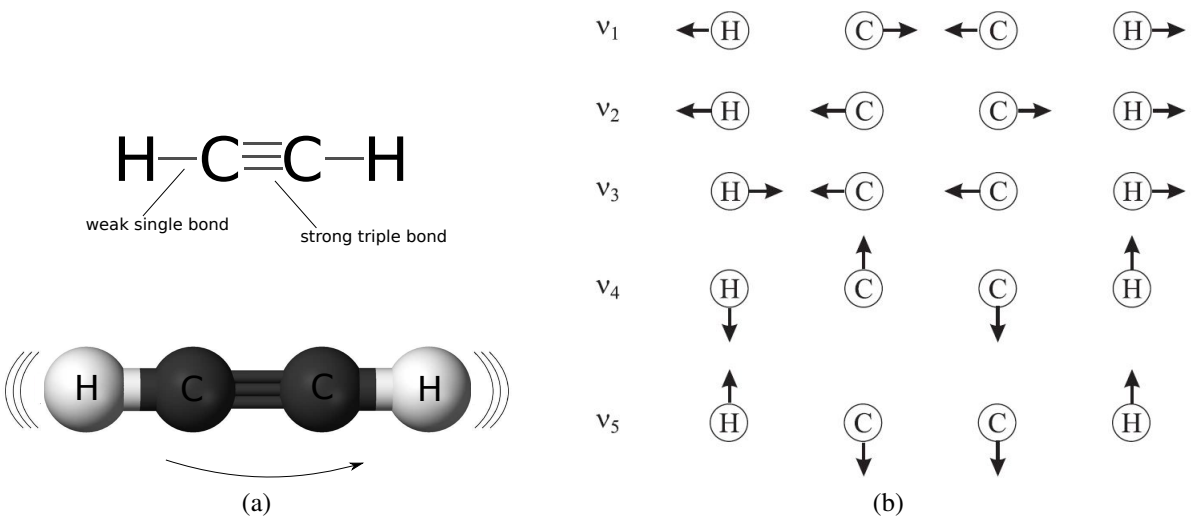

Figure 4: (a): The acetylene C_2H_2 structure. Strong triple bond between the C atoms and single bond between the C and the H atom. The acetylene molecule can vibrate and rotate. (b): The different vibrational modes for the acetylene molecule noted with the vibrational quantum number ν. Figure from [1].

When the interaction is not linear we have a combination of the different vibrational modes, e.g., the modes coupled $\nu_1 + \nu_3$. Transitions from this combination can be used as a frequency reference, since the strong lines in the ro-vibrational combination band are very narrow. The infrared region from 1530 nm to 1560 nm, is the dominant region for long-distance telecommunications and optical metrology. The acetylene molecule provides a large number of reference transitions coincident with the telecommunication band.

However not all transitions are allowed and there are certain selection rules to be followed. The selection rule for the rotational J operator is $\Delta J = J' - J'' = 0, \pm 1$ where the J' stand for the final energy state and J" for initial energy state. For each of the allowed values of ΔJ, the transitions are divided into three branches. If $\Delta J = 1$ the transitions are in the "R-branch", and if $\Delta J = -1$ the transitions are in the "P-branch" and when $\Delta J = 0$ the transitions are in the "Q-branch". Transitions between ro-vibronic states are noted as $P(J'') : \nu' - \nu''$ and $R(J'') : \nu' - \nu''$. See figure 5.

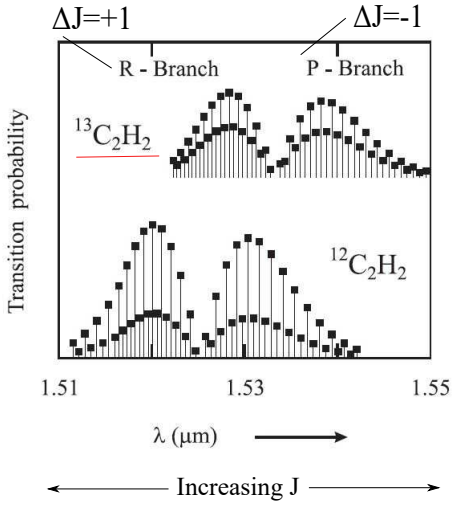

Figure 5: The transition bands for the acetylene molecule C_2H_2 with the transition probability as a function of the wavelength. The P and R-branch for the acetylene molecule can be seen. The energy separation for the P and R-branch changes with increasing rotational quantum number J. Note that the transition probability is not much higher for $^{13}C_2H_2$ than $^{12}C_2H_2$. Figure from [1].

The rotational bands, P and R-branch for the acetylene molecule can be seen in figure 5 where the transition probability is shown as a function of the wavelength in μm. For every ro-vibrational transition depending on ΔJ, gives rise to certain wavelengths and the modes can be observed. The transition of interest in this project is the ro-vibrational transition noted as $P(16) : \nu_1 + \nu_3$. The transition is in the P-branch and this means that $\Delta J = -1$ and that $J' - J'' = 15 - 16 = -1$. So the rotational energy level changes from level 16 in the ground electronic state to level 15 in the excited electronic state. The vibrational state is a combination of the ν_1 and ν_3 modes which can be seen in figure 4 (b). Within a given rotational or vibrational energy level, the lower state populations are usually described by the population probability. Under thermal conditions, these are given by the Boltzmann distribution. Within a given Boltzmann constant the population probability is temperature dependent, thus the probability for a ro-vibrational transition to take place.

3 Broadening mechanisms and line shapes

In the real world when measuring these transitions, they are not described by a delta function or not precisely ”sharp”. The excited state have a finite lifetime and therefore a finite width of the absorption profile that is a measure of how likely it is for the particle to absorb the photons as a function of the frequency of the light.

From the uncertainty principle we find that the linewidth of the transition can be expressed in terms of life time of the particular state:

$$\Gamma \sim \frac{\hbar}{\Delta t} \tag{8}$$

where the Γ is expressed as the ”natural line width” and Δt is the lifetime. This broadening arises from the uncertainty in the energy states in transitions. The absorption profile for the natural line width is described with a Lorentzian line shape function or Lorentzian distribution. The probability density function of the Lorentzian can be expressed as,

$$L(\omega) = \frac{1}{\pi(\Gamma/2)} \left[\frac{(\Gamma/2)^2}{(\omega - \omega_0)^2 + (\Gamma/2)^2} \right] \tag{9}$$

where the ω_0 is the location parameter of the peak and also the resonant angular frequency of the transition. $\Gamma/2$ is the Half-Width at Half Maximum (HWHM).

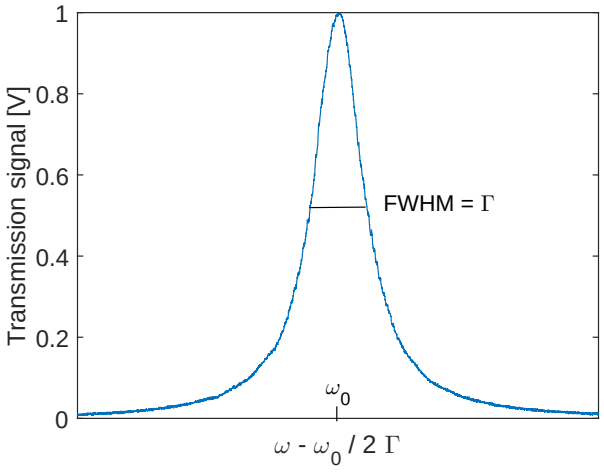

Figure 6: The Lorentzian lineshape function $L(\omega)$ near resonant absorption with the natural linewidth Γ. The Lorentzian function is normalized so that $\int_{-\infty}^{+\infty} L(\omega) = 1$

But there are several other broadening effects that come into play when measuring the transmitted signal from a sample of interest thus broadening of the measured linewidth of the transition. One of them is the *Doppler effect* where the velocity of the atoms or molecules play an important role. In general there are two kinds of broadening effects: homogeneous and inhomogeneous broadening mechanism. The homogeneous broadening effects affects the radiating or absorption of the atoms or molecules equally. An example of this is the natural line width. The inhomogeneous broadening effects are those where each atom or particle interacts with the radiation in a different way because this depends on the velocity of the individual atoms or particles. An example of this is the *Doppler broadening effect*.

3.1 Doppler broadening

When the atoms or molecules have a non-zero velocity and they move towards the observer the emitted radiation will be shifted to higher frequency. When the atoms or molecules are moving away from the observer the emitted radiation will be shifted to lower frequency. The Doppler shift in frequency will be given by the angular frequency ω_0 of the radiation in the laboratory's frame of reference and the angular frequency seen in a frame of reference moving with a certain velocity v [4, p.151],

$$\omega = \omega_0 \pm kv \tag{10}$$

where the wavevector is given by $k = \omega/c = 2\pi/\lambda$.
Atoms moving with velocity v absorb radiation when $\omega - \omega_0 = kv$ and the Doppler broadening is given by,

$$\frac{\omega - \omega_0}{\omega_0} = \frac{v}{c} \tag{11}$$

The velocity of the atoms moving in a gas can be described by the Maxwell Boltzmann distribution,

$$f(v)dv = \sqrt{\frac{M}{2\pi kT}} exp\left(-\frac{Mv^2}{2kT}\right)dv = \frac{1}{u\sqrt{\pi}} exp\left(-\frac{v^2}{u^2}\right)dv \tag{12}$$

where $u = \sqrt{2kT/M}$ is the most probale speed, m is the mass of the particle, T is the temperature and k is the Boltzmann constant.

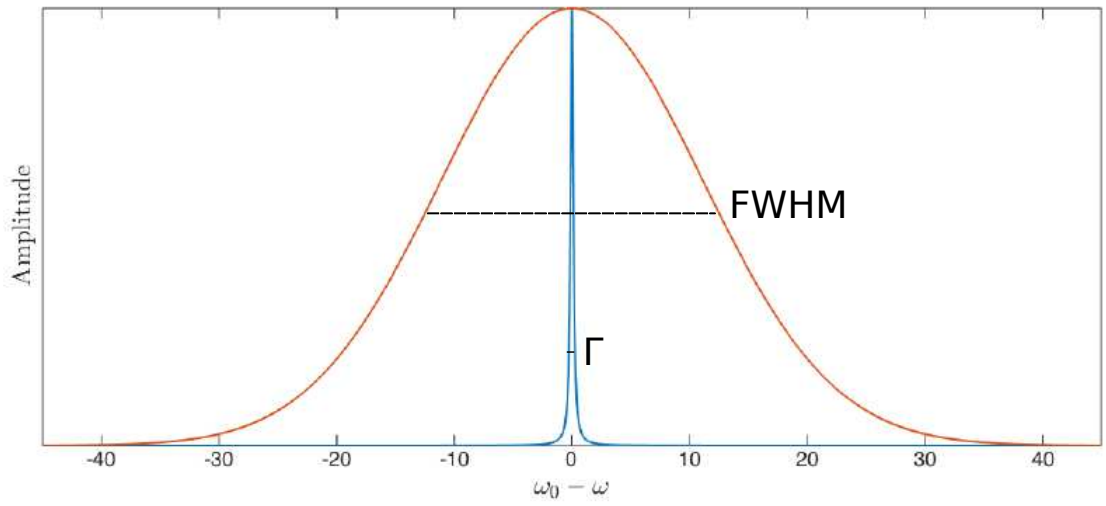

Figure 7: The Doppler broadened absorption profile with the FWHM. The natural linewidth for a transition is often much smaller than the FWHM of the Doppler broadened profile. Figure from [5].

The absorption has a Gaussian line shape function which is given by,

$$g_D(\omega) = \frac{c}{u\omega_0\sqrt{\pi}} exp\left(-\frac{c^2}{u^2}\left(\frac{\omega-\omega_0}{\omega_0}\right)^2\right) \tag{13}$$

The Full-Width at Half Maximum (FWHM) for this function is given by,

$$\Delta\omega_{FWHM} = \sqrt{\frac{8kT\ln(2)}{mc^2}}\omega_0 \tag{14}$$

The line width of the Doppler broadened function is in most cases much wider than the natural line width. See figure 7. The Doppler broadening will be more dominant for larger speeds of the particles. This broadening mechanism can be reduced by decreasing the temperature of the gas therefore reducing the velocity of the particles. There are different methods for reducing this broadening effect, one of them is the *saturated absorption spectroscopy* or Doppler-free spectroscopy. This method overcomes the Doppler-broadening without decreasing the temperature of the absorbing sample and will be used in this project. This will be explained more in detail in section 4.3.

3.2 Voigt profile

As the Doppler effect can not be neglected, a convolution of a Lorentzian and Gaussian profile yields a so-called *Voigt profile*. The Voigt profile is normalized and can be expressed as,

$$V(\omega;\sigma,\Gamma/2) = \int_{-\infty}^{+\infty} G(\omega';\sigma)L(\omega-\omega';\Gamma/2)d\omega' \tag{15}$$

where ω' is the shift from the line center, $G(\omega';\sigma)$ is the centered Gaussian profile. The probability distribution of the Voigt profile is given by,

$$\varphi_f(\omega;\sigma,\Gamma/2) = a\cdot\left(e^{-\sigma^2(\omega-\omega_0)^2/2-(\Gamma/2)|\omega-\omega_0|}\right) + y_0 \tag{16}$$

where ω_0 is the position of the peak, a is a scaling factor, σ^2 is the variance from the Gaussian profile and $\Gamma/2$ is the Half-Width at Half Maximum for the Lorentzian profile. The Full-Width at Half Maximum for the Voigt function is given by,

$$FWHM_v = 0.5346\cdot FWHM_L + \sqrt{0.2166\cdot FWHM_L^2 + FWHM_G^2} \tag{17}$$

where the $FWHM_L = 2(\Gamma/2)$ for the Lorentzian profile and $FWHM_G = 2\sigma\sqrt{2\ln(2)}$ for the Gaussian profile. Equation 17 is an approximation with an accuracy of 0.02 % [7].

3.3 Collisional broadening

The particles in a gas are moving with a certain velocity v they tend to collide with each other. This gives rise to the collisional broadening also called the *pressure broadening*. The absorption process is interrupted by collisions with other molecules and the effective lifetime of a transition is shortened thereby a broadening of the Lorentzian line profile. The collisional broadening becomes stronger when the pressure of the gas increases [6]. In this project the absorption molecules are at room temperature and the pressure of the molecules inside the glass cell is believed to be approximately 1.1 Pa. The pressure broadening is the dominating broadening mechanism in this project.

3.4 Power broadening

When the molecules experience high intensity or electromagnetic radiation, it will lead to an increase in the rate of absorption and stimulated emission until it's greater than the rate of spontaneous emission. So the beam keeps exciting the system and this leads to a saturation of the system. Power broadening also known as *saturation broadening* is the broadening of the resonance at high intensities of the laser beam. The absorption profile for the power broadening has a Lorentzian line shape with a Full-Width at Half Maximum (FWHM) given by,

$$\Delta\omega_{FWHM} = \Gamma\left(1 + \frac{I}{I_{sat}}\right)^{1/2} \tag{18}$$

where the Γ is the natural line width and the I_{sat} is the saturation intensity. The width of the profile goes as the square root of the intensity. In our case by increasing the laser power, the power inside the cavity will also increase and the transmission signal will be maximised. However the linewidth of the saturated absorption signal will be broadened. The power broadening is one of the dominant broadening mechanism in this project.

3.5 Transit time broadening

When the absorbing molecules with a certain velocity interacts or goes through the interrogating beam of light the transit time will be determined by the speed of the absorbing molecules and the beam waist of the light field,

$$\Delta t = \frac{2w_0}{v} \tag{19}$$

where Δt is the transit time and w_0 is the waist radius of the beam. The transit time broadening is a lifetime limited broadening and is inversely proportional to the waist size of the beam,

$$\Delta\nu_{transit} = \frac{v}{2w_0} = \frac{1}{2\pi}\sqrt{2\ln(2)}\sqrt{\frac{\pi k_B T}{2M}} \cdot \frac{1}{2w_0} \tag{20}$$

where v is equal to the Maxwell Boltzmann distribution of the most probale speed of the molecules, k_B is the Boltzmann constant, M is the mass of the molecule and T is the temperature.

In our case, the absorbing molecular sample is the acetylene molecule. The transit time broadening can be calculated. The temperature of the acetylene molecules are at room temperature T = 300 K. The waist radius is calculated to be $w_0 = 0.75$ mm for our cavity. The waist radius of the beam is expressed in section 4.2. The transit time broadening is calculated to be $\Delta\nu_{transit} = 48.45$ kHz. The most dominant broadening mechanisms are the pressure broadening and the power broadening by a factor of 20.

4 Experimental setup, method and techniques

The experimental setup is described in figure 8 and in this section we will discuss the entire setup and different techniques used in this project. A short list of all the different components used in the experimental setup are described. Some of the components are not mentioned in the experimental setup in figure 8, but will be used and discussed in later sections.

► **Mirrors:** The mirrors reflects the light and shape the beam.
► **Lenses:** The lenses are used to adjust the beam size and collimate the beam for mode matching.

►**PD - Photodetector:** detects the transmission of light, e.g, from the cavity.
►**PBS - Polarizing beam splitter:** an optical device that splits the light into two separate s- and p-polarization components by reflecting the s component with the dielectric beamsplitter coating, while allowing the p component to pass.
►**λ/2 - plates:** This device will rotate the polarization direction of the polarized light going through the plate.
►**Beam splitter:** This device will split the light into two separate beams.
►**PZT - Piezo eletric crystal:** This component is located on one of the mirrors in the cavity. By applying voltage over the crystal, an expansion of the crystal will occur. This will vary the length of the cavity on the scale of nm to µm
►**Free-space isolator:** This prevents backreflections into the fiber laser. It is an optical component which allows the light to go only in one direction. The free-space isolator consist of a Faraday rotator and two PBS. This device is designed for light in the infrared wavelength range.
►**EOM - Phase modulator**: Used to generate sidebands by making a variable phase shift on a linearly polarized input beam .
►**PID controller:** A proportional–integral–derivative controller is a control loop feedback system which corrects an error value e(t) based on the input of the three terms: the proportional term K_p, the integral term K_i, and the derivative term K_d. The corrected output error value is sent back to the piezo electric element located on the input mirror of the cavity.
►**DBM - Double Balanced Mixer:** A circuit where two input signals at frequencies ω_1,ω_2 are applied into the mixer. The frequency of the two signals will be multiplied. This is called ”beating” of the frequency signals. The mixer output produces a new signal at the sum and difference of the frequencies.
►**RF Bandpass filter:** an electronic device that allows signals between two specific frequencies to pass.

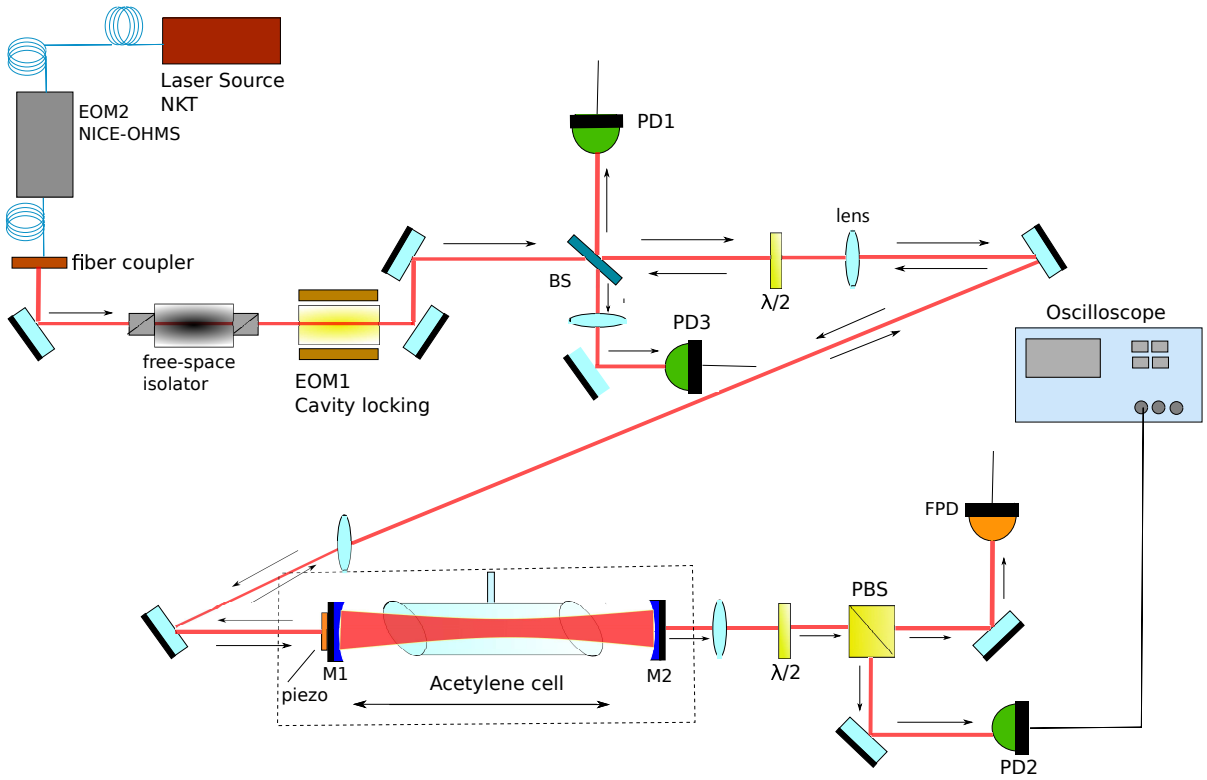

Figure 8: The experimental setup. Beam splitter (BS). Photo detector (PD1) for detection of the reflected light. Electro-Optic-Modulator (EOM1) for cavity locking and (EOM2) for NICE-OHMS technique. Photo detector (PD3) for RAM stabilization. Polarizing beam splitter (PBS). Photo detector (PD2) for the transmitted light from the cavity. Fast photo detector (FPD) for molecular phase detection (NICE-OHMS).

The laser source is an Erbium doped fiber laser which delivers light at ~ 1542.37 nm. The light enters a fiber coupler. The free-space isolator will prevent the light to be reflected back into the fiber. The light is then beam shaped by the mirrors and lenses. The beam splitter (BS) split the light into two separate beams, one travelling into the (PD1) detector which is a photo detector for cavity stabilization and detects the reflected light from the cavity. The other beam into the (PD3) detector for RAM stabilization. This will be discussed more in detail in section 4.5. The (EOM1) create sidebands and modulate the laser light before the light enters the cavity and the modulation frequency is around 10-20 MHz. The (EOM1) is used for Pound-Drever Hall locking scheme in order to lock the cavity to the laser frequency. The generated error signal is fed into a piezo-electric element located on the input mirror M1. The transmitted light from the cavity is then separated into two paths using a polarizing beam splitter (PBS). PD2 measures the transmission signal, the light transmitted from the cavity which is then coupled to the oscilloscope. The (EOM2) is for the NICE-OHMS signal creates another pair of sidebands equal to the cavity's FSR. The free-spectral range in our cavity is around FSR = 500 MHz. A fast photodetector (FPD) detects the NICE-OHMS phase signal. The saturated absorption signal is monitored by the PD2 detector.

4.1 The laser

The laser we are using in this experimental setup is an Erbium doped fiber laser from NKT photonics. The laser delivers light about 1542.37 nm. The frequency of the laser can be tuned by adjusting the voltage sent into the built-in piezo, the temperature and power can be controlled by the computer. The laser power can deliver up to 48 mW IR power and the desired power can be adjusted by the computer. A triangle wave is applied to the built-in piezo inside the laser. This way we can adjust the

frequency and amplitude of the triangle wave. By adjusting the amplitude of the triangle wave, the range of the scan can be varied, observed from the oscilloscope.

When light enters the (EOM2), we have a certain amount of loss which is around 50 % (3 dB). This means the amount of laser light power is reduced when travelling through the (EOM2). The coupling efficiency can be measured from the photo detector PD1, the amount of light coupled into the optical cavity. An estimate of the coupling efficiency can be made on the oscilloscope.

4.2 Optical cavity

An optical cavity or resonator consists of two reflecting mirrors facing each other and separated by a distance L, forming standing waves for light. Each mirror has a reflection and transmission coefficient, for the input mirror M_1 we have r_1,t_1 and for the output mirror M_2 we have r_2,t_2. These coefficients determines how much of the incident light is transmitted or reflected. The input power is given by P_0 or P_{in} and the intra-cavity power P_c and the output power P_{out}, see figure 9. The intra-cavity power is much higher due to the repeated reflection of light inside the cavity that gives rise to an increased intensity.

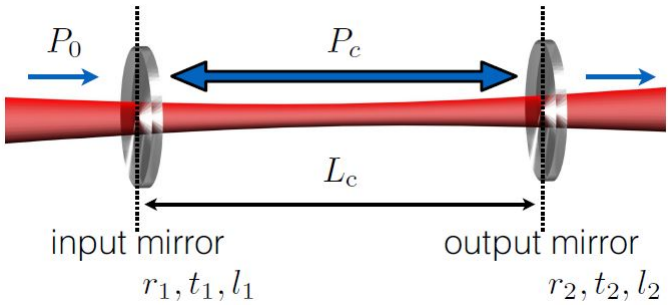

Figure 9: Figure from [6]. A Fabry-Pérot cavity with an input and output mirror. The length of the cavity L_c i.e. distance between the mirrors in our setup is approximately 30 cm. Each mirror has a reflection and transmission coefficient given by r_1, t_1 and r_2, t_2. But each mirror also has losses which is given by l_1 and l_2. The cavity, input and output power are shown.

An optical cavity can support constructive interference only for certain frequencies that fulfills the condition,

$$L = m\frac{\lambda}{2}, \quad m = 1, 2, ... \tag{21}$$

where L is the length of the cavity, λ is the wavelength of the light and m is a positive integer.
This means that only certain frequencies can exist inside the cavity and all other frequencies will interfere destructively. These frequencies are called modes. The spacing between the resonator modes is defined as the Free-spectral range (FSR) of the optical cavity.
Another fundamental parameter which describes the quality of an optical cavity is the *Finesse* and can be calculated as the ratio of Free-spectral range (FSR) and Full-Width at Half Maximum width of the resonator mode,

$$F = \frac{FSR}{FWHM} = \frac{\pi\sqrt{r_1 r_2}}{1 - r_1 r_2} \tag{22}$$

where $r_1 r_2 = R$ the reflection coefficients.

The finesse can also be determined by the the losses. The loss for the cavity can be described by $Loss = 2(T + A)$ and we get,

$$F = \frac{2\pi}{Loss} = \frac{\pi}{T + A} \tag{23}$$

where T and A is the per mirror power transmission and loss. If an absorption cell is placed within the cavity, the amount of loss can be expressed as,

$$Loss = T_1 + T_2 + L_{cell} \cdot \alpha \cdot p \tag{24}$$

where α is the C_2H_2 absorption coefficient $\alpha = 6,93 \cdot 10^{-3}$ m^{-1} Pa^{-1} the P(16) transition line [8]. The cell length is given by $L_{cell} = 15$ cm and the pressure, $p = 1.1$ Pa. The transmittance is given by $T_1 = 1 - R_1 = 1 - 0.986 = 0.014$ and $T_2 = 1 - R_2 = 1 - 0.999 = 0.001$. See figure 8.

The finesse is inversely proportional to the lifetime of the photons in the cavity. The photons have a limited lifetime inside the cavity due to the transmission of the cavity mirrors and random scattering. The finesse is also related to the quality factor Q which is given by the ratio of the resonant optical frequency to the cavity linewidth. This factor describes the loss per period of an oscillator and by achieving a high Q factor we'll get low loss per round trip.
The Free-spectral range (FSR) for our optical cavity is approximately 500 MHz and the length of the cavity $L_c = 30$ cm. The reflection coefficients are given for each mirror $R_1 = 0.986$ and $R_2 = 0.999$ and the radius of curvature 9 m for both mirrors. The approximated maximum finesse can be estimated by using equation (24) we get,

$$F = \frac{2\pi}{Loss} = \frac{2\pi}{0.014 + 0.001 + (6.93 \cdot 10^{-3} m^{-1} Pa^{-1} \cdot 0.15m \cdot 1.1Pa)} = 389.20 \tag{25}$$

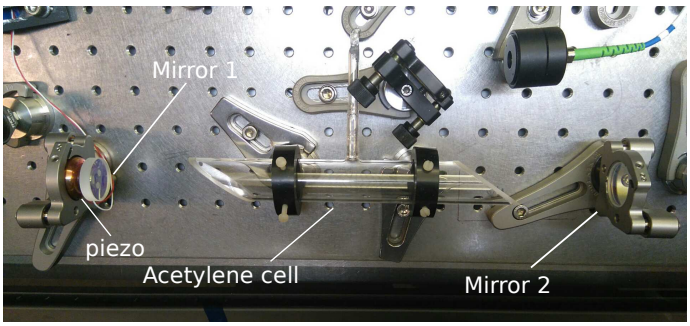

Figure 10: Our Fabry-Perot cavity with the acetylene cell within.

The piezo electric element expands when voltage is applied and is placed on the input mirror. This will stabilise the cavity, maximising the transmission signal, see figure 10. The finesse can be calculated experimentally by scanning the cavity length with the piezo electric element. The FWHM of the cavity resonant mode and the FSR of the two modes in the cavity can be measured from the cursor measurements on the oscilloscope. Equation (22) can be used. When measuring the transmission signal from the photo detector PD2, the signal is not a function of the frequency but the piezo position as we vary the voltage sent into the piezo. The unit can be converted to frequency by using the error signal generated using PDH-technique, this will be discussed more in detail in section 4.4. Data collected for measurement of the finesse of our cavity can be seen in figure 11. In this project we have used the oscilloscope cursor measurements to measure the FSR and the FWHM, this method yields only an estimate of the finesse. The uncertainty by using the cursor measurements on the oscilloscope is around 1 %. The variation in the position by the piezo electric element is also assumed to be small.

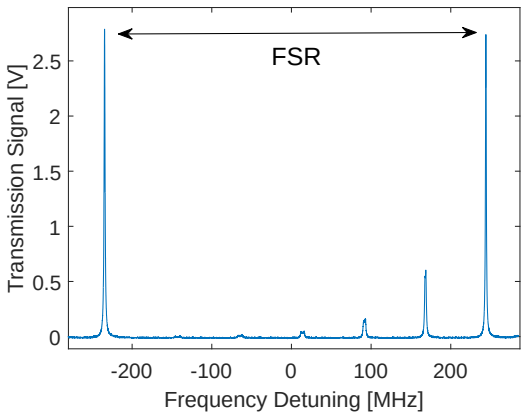

(a) Measuring the finesse of the cavity by tuning the range of the scan for a whole FSR.

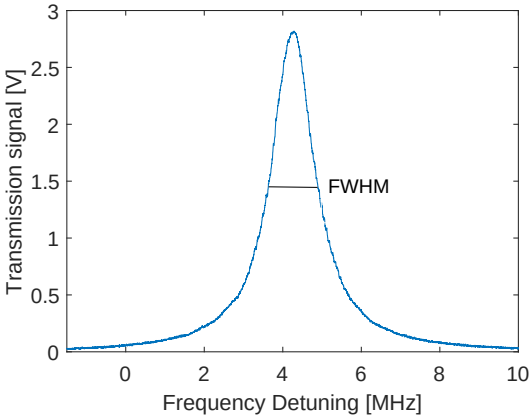

(b) Measuring the FWHM of the resonant frequency of the cavity

Figure 11: Data collected for the transmission of the cavity by scanning the length of the cavity. The length was varied by the voltage sent into the piezo element on the input mirror. The transmission signal is measured in volts. The absorption cell is placed within the cavity. The finesse of this alignment is measured to be $F \approx 333.75 \pm 3.33$. *The measured coupling efficiency around 50.9 %*

The Brewster cut windows also introduces an amount of loss. If they are not being cleaned they can scatter the photons randomly and reduce the finesse. The cavity will enhance the effective interaction length between the laser light and the absorption cell by a factor of $2F/\pi$. When the laser light is coupled into the optical cavity the beam profile must match the mode supported by the cavity. The waist diameter of the beam $2\omega_0$, has to be the same as the waist diameter of the cavity. This is called mode matching. The waist radius of the beam in the cavity is determined by the radius of curvature of the mirrors in the optical cavity and the cavity length. This can be expressed as,

$$w_0 = \sqrt{\frac{\lambda}{\pi}}\left[\frac{L}{2}\left(ROC - \frac{L}{2}\right)\right]^{1/4} \tag{26}$$

where L is the length of the cavity, λ is the wavelength of the laser light, ROC is the radius of curvature of the mirrors. The waist radius of the beam for this project is calculated to be $w_0 = 0.75$ mm.

The absorption cell used in this project is in gaseous form placed inside a glass cell. The cavity will enhance the effective length of the sample by a factor of $2F/\pi$ so the sample pressure can be reduced. The pressure of the acetylene cell in our experiment is believed to be approximately 1.1 Pa.

4.3 Saturated absorption spectroscopy

To reduce the Doppler broadening without cooling down the absorbing sample to much lower temperatures, a more general pump-probe beam method can be used. A laser is sent through an absorbing sample, this is the pump beam. Another counter-propagating beam known as the probe beam with the same frequency as the pump beam is also sent through the absorbing sample with opposite direction. The two beams are at the same frequency but they interact the with each molecule differently because of the motion of the molecules. If the frequency of the laser is red-detuned with respect to the transition frequency, the pump beam will absorbed by the molecules moving towards the beam source and the probe beam will be absorbed by molecules moving away from the beam source. If the frequency of the laser is blue-detuned the opposite will occur.

When the frequency of the laser is tuned to resonance, both beams will be absorbed by the same molecules, those with velocities perpendicular to the direction of the laser beam. The strong pump

beam will excite these particles and when the probe beam interacts with the molecules it will experience less absorption since the particles already have been excited. The signal will be detected by a photo diode and when sweeping across the resonance a small peak or dip will be seen in the bottom of the Gaussian Doppler broadened absorption profile of the probe beam. The small peak or dip is called the ”Lamb dip” or ”hole burning” in the absorption. If the pump beam is stronger, i.e, higher intensity, the power broadening of the width of the Lamb dip can be seen. The width or FWHM of the Lamb dip can approach the natural linewidth of the transition. The width is much smaller than the width of the Gaussian profile. See figure 12.

Saturation absorption spectroscopy in this project is done by using Cavity Enhanced Absorption Spectroscopy (CEAS). The method is to place an absorbing sample inside an optical cavity and the light inside the cavity will pass the absorbing sample multiple times due to the repeated reflection of the light from the cavity mirrors. The absorbing molecules will be saturated by the beam. When using CEAS the effective interaction length in the cavity will be enhanced.

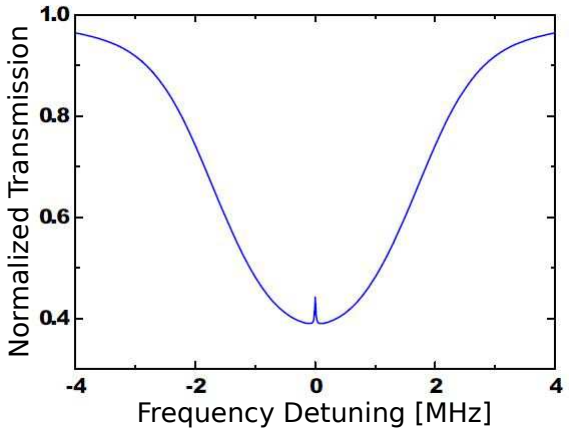

Figure 12: Figure from [9]. A illustrated Gaussian Doppler broadened transmission profile with the small peak signal obtained from saturated absorption spectroscopy.

The saturation absorption spectroscopy in this experiment was observed by scanning the cavity length and locking the cavity resonance to the laser frequency. The three input terms from the PID-controller can be adjusted by the computer which corrects the error value e(t) sent back into the piezo electric element located on the input mirror for the optical cavity. The optical cavity will then be locked to the desired mode. By sweeping over the frequencies we were able to observe saturated absorption signals in a Doppler broadened profile. The data collected can be seen in figure 13. The linewidth from the observed saturation signal peak can be measured by fitting with a Lorentzian profile. The input laser power sent into the cavity was varied and the output power from the cavity was also measured. Saturated absorption signals for different input laser powers 20-48 mW were observed and data were collected. In section 5 we will discuss the relation between the linewidth of the saturated absorption peak and the intra-cavity power.

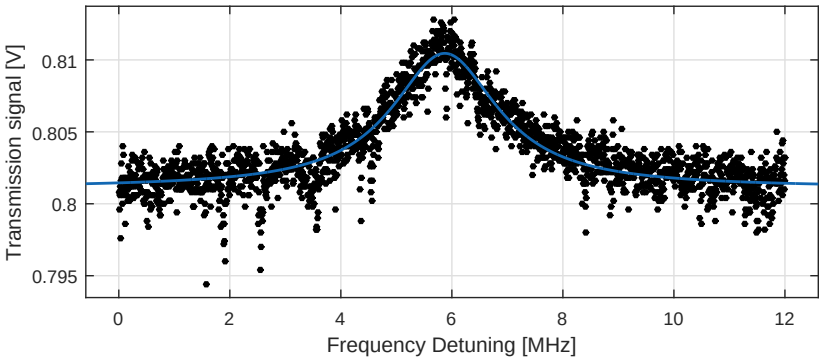

Figure 13: Data collected of saturated absorption peak for 40 mW laser power. The Lamb dip is fitted with a Lorentzian profile. The linewidth of the peak is measured to be 2.26 ± 0.12 MHz.

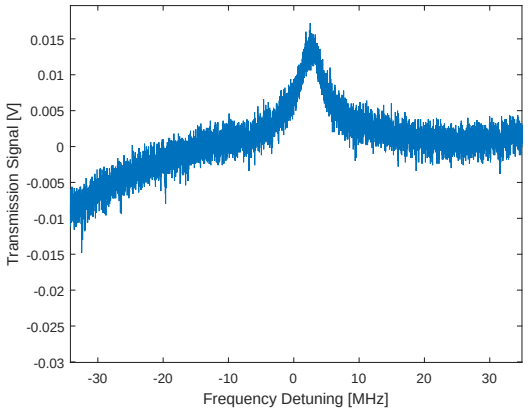

(a) No low-pass filter was connected here. The noise contributed in collected signal can be observed. Linewidth of the peak measured to be 2.01 MHz.

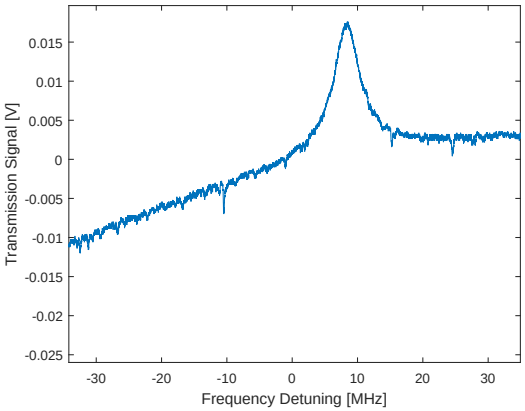

(b) A low-pass filter was connected in this setup right before the signal was connected to the oscilloscope. This will reduce additional noise present in the saturated absorption peak. The linewidth of the peak is measured to be 1.80 MHz.

Figure 14: Data collected for saturated absorption signals with 800 mW intra-cavity power. The linewidths are measured by fitting to Lorentzian profile. Both signals are measured with the same alignment.

4.4 Pound-Drever-Hall (PDH) technique

The Pound-Drever-Hall (PDH) technique was described by R. V. Pound, Ronald Drever, and John L. Hall in 1983. This powerful technique is a phase modulation spectroscopic method which is used to stabilise the frequency of a laser to an optical cavity. An error signal is generated using this technique. The reason that we need standing wave all the time in the cavity, is to make sure that light gets transmitted through the cavity and through the sample placed inside the cavity. An error signal is important in order to control a given system, and how far from the desired state a given system is, due to vibrations and thermal fluctuations that can disrupt the conditions for a stable cavity.

The Pound-Drever-Hall technique depends on the frequency modulation of the light coupled into the cavity and the reflected light from the cavity. Our laser has a frequency ω, and is modulated with an Electro-Optic-Modulator (EOM) to create sidebands with frequencies $\omega - \omega_m$ and $\omega + \omega_m$. The carrier signal plus two small sidebands. See figure 15. The EOM consists of an electro-optical crystal placed in between two metal plates which works as a capacitor. By applying a sinusoidal voltage into

the EOM thus into the crystal, the index of refraction of the crystal will change. The crystal inside the EOM1 used in this technique, is larger than the crystal inside the EOM2 for the NICE-OHMS technique. When the crystal is smaller the two metal plates are closer to each other and the electric field for the capacitor will be larger. This will cause the EOM to create sidebands at much higher frequencies. But the EOM1 used in this technique will only modulate the light in the region 10-20 MHz. By using an EOM we can generate sidebands with a well defined separation frequency with respect to the carrier frequency. The sinusoidal voltage or the modulation frequency can be adjusted from a function generator. This is used in this experimental setup.

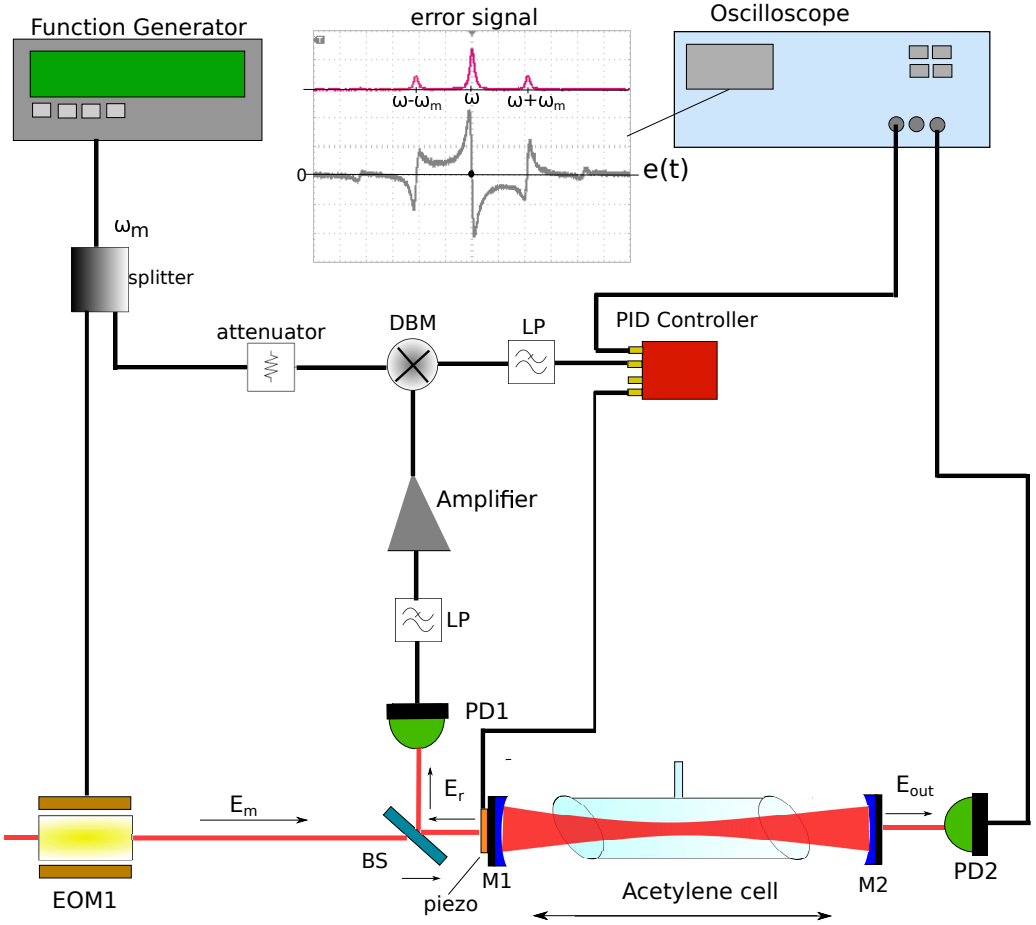

Figure 15: The experimental setup for the Pound-Drever-Hall technique. The modulation frequency ω_m is generated by the function generator. This modulation frequency is split and one is applied to a double-balanced mixer (DMB) and the other to an EOM. The reflected signal from the cavity is detected by the photo diode, PD1. The light transmitted from the cavity is detected by the photo detector, PD2 which is further coupled to the oscilloscope. The reflected light signal detected by PD1 is sent through to a 11 MHz low-pass filter (LP). The signal is then amplified and applied into a double-balanced mixer (DBM). The reflected signal is mixed with the modulation frequency generated by the function generator. The reflected signal is demodulated with the modulation frequency ω_m. The output signal from the DBM is coupled to the PID-controller. The output signal from the PID-controller is coupled to the oscilloscope. The reflected field is denoted in this figure as E_r, the modulated field E_m and the output field from the cavity E_{out}.

The error signal is generated by detecting the reflected light from the cavity. See figure 15. The signal detected by the photo diode generates a photocurrent that is proportional to the square of the electric field. If the frequency of the laser drifts out from the resonance, we can't tell from a symmetric absorption signal whether the frequency needs to be increased or decreased to bring it back to resonance. The derivative of the reflected signal is antisymmetric around cavity resonance. This

signal can be used as an error signal to lock the optical cavity to the laser frequency. The modulation phase of the reflected beam and the modulation frequency coupled into the DBM, can be adjusted by varying the modulation frequency. The output of the DBM is the product of the two inputs, so the output will contain signals at both low frequency and twice the modulation frequency. We are interested in the low frequency, since this will tell us the derivative of the reflected beam. Therefore a low-pass filter is connected on the output of the DBM so the low frequency signal can get through and further into the PID-controller.

When the cavity is on resonance with the carrier frequency, the carrier frequency will be phase shifted 180°, the two beams interfere destructively and the total reflected beam vanishes. But if the cavity is not quite on resonance with the carrier frequency then the phase difference will not be exactly 180° and they will not cancel each other.

The error signal is zero at carrier frequency resonance. This is the desired point for our system. The error signal can be described by the A(ω) term, and the dispersive term, $D(\omega)$. The desired error signal in this project is the dispersive term. The A(ω) component can be used to convert the units of the x-axis to Hertz. The error signal is a function of the detuning from cavity resonance. The generated error signal is connected to the PID-controller which adjust the error signal and the voltage sent into the piezo electric element for the cavity. This will lock our cavity to the desired mode.

4.4.1 The collected PDH signals

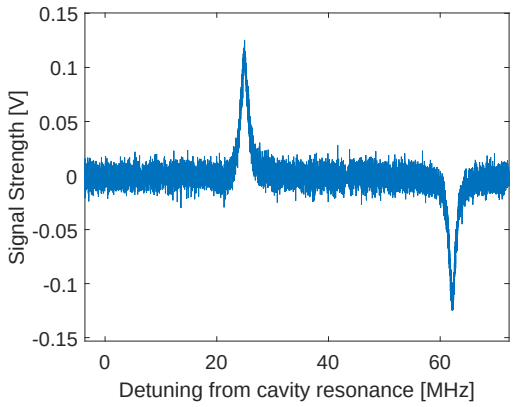

(a) The A(ω) component of the PDH signal with modulation frequency ω_m = 18.6 MHz

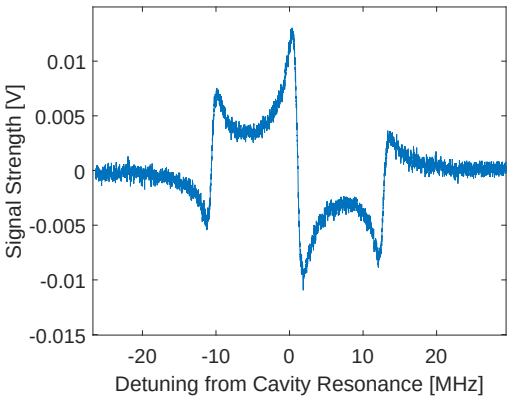

(b) The dispersive component $D(\omega)$ with the modulation frequency ω_m = 11.9 MHz

Figure 16: Collected Pound-Drever-Hall error signals. The A and D components of the error signal strength measured in volts as a function of the detuning from cavity resonance.

4.5 NICE-OHMS technique

The NICE-OHMS measurement technique stands for Noise Immune Cavity Enhanced Optical Heterodyne Molecular Spectroscopy. When performing NICE-OHMS measurements it is the transmitted light that is measured and the most interesting. The light is transmitted through the cavity this signal will contain noise arising from vibrations and fluctuations of the cavity mirrors. The NICE-OHMS technique is used in order to lower the noise of the phase shift signal of the light interacting with the sample. But in general in order to lock a laser frequency to an atomic or molecular transition we need an error signal, e.g, the phase shift around resonance. When the field of the laser interacts with the field from the sample, it will generate a phase shift that we want to measure.

In our system the light is modulated with an EOM at a frequency equal to the cavity FSR before entering the cavity. The separation of the modes or the FSR of our cavity is approximately 500 MHz. By adding light into the cavity that is modulated with modulation frequency $\Omega = FSR = 500$ MHz it will sample the same noise as the carrier yet be unaffected by the sample, and at the same time enhance the signal. Only the laser frequency, i.e, the carrier frequency will interact with the molecular resonance. In our setup, the carrier frequency is scanned across the cavity and the molecular resonance. The cavity resonance mode is locked to the laser frequency, see figure 17.

The modulation frequency is split by a splitter. One signal is coupled to a coupler and then amplified by an amplifier, and further into the EOM2 that generates sidebands at the modulation frequency. The modulation frequency signal is also connected to a DBM. The transmitted signal from the cavity is detected by a fast photodetector (FPD) and passed through a RF bandpass filter which filters out frequencies higher than 500 MHz. This signal is fed into the DBM and is demodulated with the modulation frequency. The DBM is then connected to the oscilloscope, see figure 17.

The other signal from the splitter is for a so-called RAM stabilization. This will be further explained, see below. The incident light after travelling through the EOM and before entering the cavity is detected by the photo detector (PD3). This signal is connected to a bandpass filter (BPF) and amplified. The detected signal is then mixed into a DBM with the modulation frequency. The detected signal is demodulated with modulation frequency Ω. The output signal from the DBM is connected to a PID-controller which corrects the error signal fed into the EOM2 for RAM stabilization.

RAM is defined as residual amplitude modulation. The EOM consist of a crystal and when voltage is applied to the crystal, the index of refraction of the crystal changes. But when the temperature of the crystal in the EOM changes, it changes the index of refraction and the way it generates sidebands. There will be an unbalance between the two sidebands, which gives rise to background signals. A reference signal is demodulated at modulation frequency, and by connecting the PID-controller, this way we can control and minimize the background signal by stabilizing the voltage fed into the EOM. The EOM2 in our project is also packed in insulating foam for passive temperature stabilization.

Both the carrier frequency and the sidebands will be resonant with the cavity modes. This means that both beams will obtain the same noise originated from the cavity. The modulation frequency or separation between the carrier and the sidebands is in the radio frequency (RF) regime. The noise from electronic devices goes as, 1/f , where f is the frequency of the detected signal. This means that noise will be eliminated since the FSR is around 500 MHz. When the two signals are mixed, the signal containing the high frequency can be filtered out by a band-pass filter and only the difference between the signals will be collected and observed by the oscilloscope. The molecular induced phase shift lies in a Doppler broadened profile. The NICE-OHMS signal detected by the fast photodetector (FPD) is phase-sensitive and this can be used as an error signal for stabilization of the laser. The saturated absorption signal discussed in section 4.3 can be monitored with the photodetector PD2 and extracted along with the NICE-OHMS signal. The collected data of the NICE-OHMS signals for 40 mW laser power are shown in figure 18.

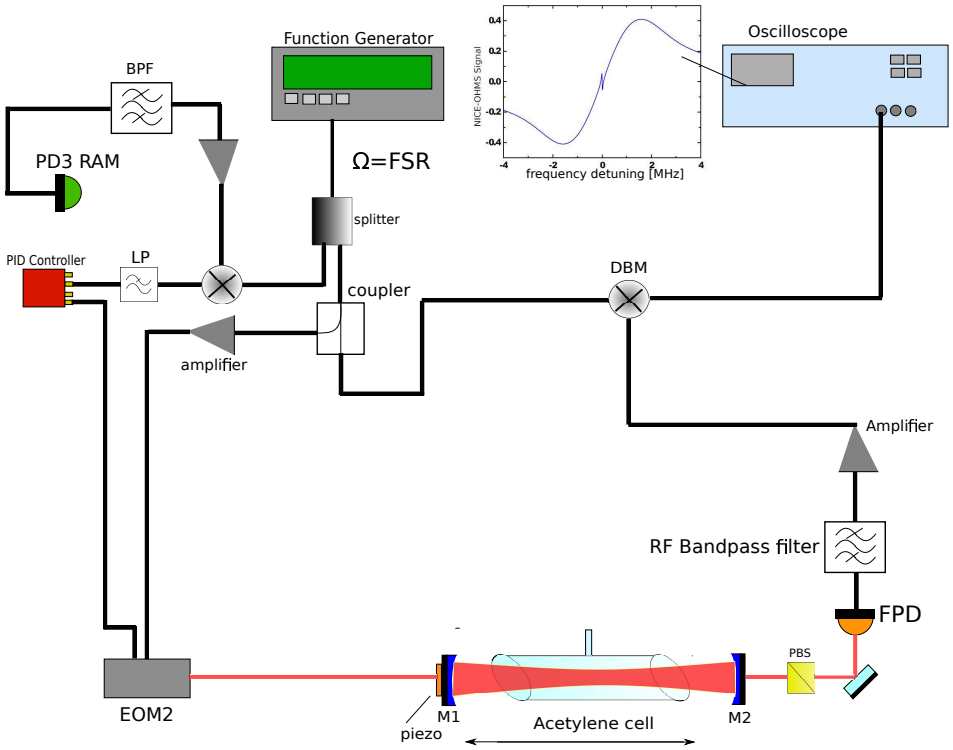

Figure 17: The experimental setup for the NICE-OHMS technique. Double-balanced mixer (DBM) for demodulation. Bandpass filter (BPF) for RAM stabilization. RF Bandpass filter for the transmission signal. Fast photo detector (FPD) for detection of the transmitted signal. Low-pass filter (LP).

4.5.1 The collected NICE-OHMS Signals

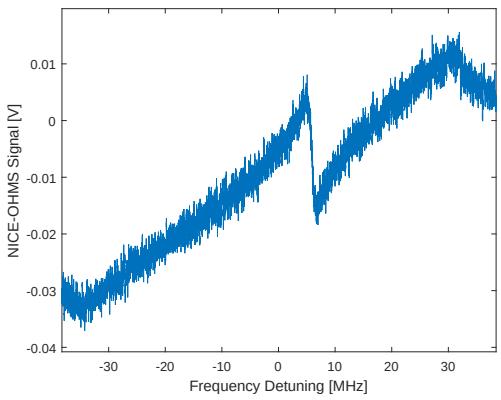

(a) collected molecular induced phase shift signal using NICE-OHMS. Signal-to-noise ratio measured to be SNR = 3.35.

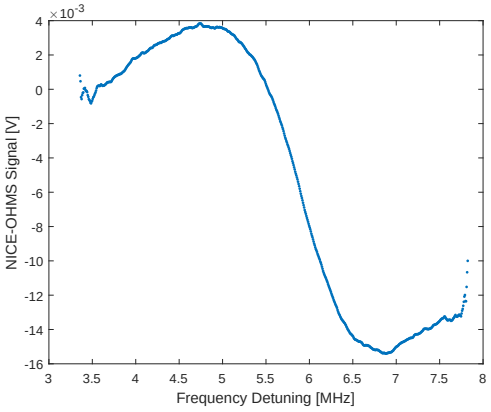

(b) This signal is obtained by smoothing over 110 points in the collected data. The width is measured to be 2.14 ± 0.06 MHz.

Figure 18: Collected NICE-OHMS signals as a function of detuning frequency in MHz. Both signals are collected for 40 mW laser power. The width of the NICE-OHMS phase shift signal is measured. The width is defined from the maximum point to minimum point of the phase shift. Both signals are from the same alignment.

4.6 The LOCK-IN Amplifier

The Lock-in amplifier use phase-sensitive detection technique, and it's a method for obtaining very small signals surrounded by a lot of noise. The lock-in amplifier, amplifies the signal and multiplies it with a lock-in reference signal. The lock-in amplifiers use a phase-locked loop to generate their own reference signal. The reference signal frequency has to be the same as the signal frequency, $\omega_r = \omega_L$. When the input signal has a frequency different from the reference frequency, the product of two will oscillate at zero. This means that noise other than the modulation frequency averages to zero

By using harmonic modulation the amplitude modulated signal is detected. Modulating the frequency near resonance frequency leads to a modulation of the signal with twice the modulation frequency 2Ω. The frequency can be expressed as, $\nu = \nu_L + \Delta \sin(\Omega t)$, where Ω the modulation frequency, and Δ the amplitude modulation.

The detected output signal can be arranged so the amplitude modulation is small and we can approximate the intensity of the signal by a Taylor series expansion. The lock-in amplifier picks out the fundamental Fourier component of this function. The derivative of the intensity is the first harmonic frequency. The second derivative is the second harmonic frequency. The lock-in amplifier locks at f, 2f (second harmonic), or 3f (third harmonic). The phase difference can be adjusted so that signal is at maximum. This can be done by the lock-in amplifier.

In this project, the cavity length was modulated, by applying a lock-in reference signal to the piezo electric element located on the input mirror of the cavity. The experimental setup can be seen in Appendix A. The collected lock-in signals of the setup used in Appendix A are shown in Appendix B. The signal-to-noise ratio is measured by the ratio of the amplitude signal and standard deviation of noise signal.

In this project another method was used by modulating the frequency of the laser directly. The function generator that generates a triangle wave for the laser, is applied into the input of a sum-amplifier. The reference sine wave signal from the lock-in amplifier is also connected to the input of the sum-amplifier. The output signal from the sum-amplifier is fed into the voltage for the built-in piezo for the laser. This means the frequency-modulated laser is scanned across the cavity resonance. The detected lock-in signals were collected and can be seen in Appendix B.

The signal-to-noise ratio is also measured of the collected lock-in signals. The first and second harmonic signals are collected for both methods. It can be observed that the signal-to-noise ratio for the second harmonic signals are relatively higher compared to the first harmonic signals. The average signal-to-noise ratio of the first harmonic generated signal is measured to be $SNR_{first} = 198.17$, and second harmonic $SNR_{second} = 364.20$, when modulating the cavity length. The signal-to-noise ratio increases significantly by a factor of 2 when modulating with twice the modulation frequency.

The average signal-to-noise ratio for first and second harmonic when modulating the frequency of the laser are measured to be: $SNR_{first} = 320.11$, $SNR_{second} = 324.94$. The difference between the ratios are significantly smaller. Only a small change in SNR can be observed. The transmission signal of the cavity resonance is extracted along with the lock-in signal. The average signal-to-noise ratio of the transmission signals are measured to be $SNR_{first} = 116.90$ and $SNR_{second} = 104.56$.

5 Experimental results and discussion

The measured data for the linewidth (FWHM) of the saturated absorption peak, with respect to the intra-cavity power measured in mW, are fitted with the power broadening profile, equation (18). The fitted results are the saturation power P_s and the natural linewidth Γ_0. The general relation between the saturation power and optical power is: $S_0 = P/P_{sat}$. Where S_0 is the saturation parameter. The saturation power depends on the linewidth of the Lamb dip and the pressure.

The measured parameters lie a little outside of the fitted line. The standard deviation over 5 measurements for various laser powers are calculated, and error bars are shown. The uncertainty of the various measurements are slightly larger. This is due to the noise contributed to the measured Lamb dip signals. Therefore making it difficult to measure the precise linewidth (FWHM) of the Lamb dip. But the data in figure 19 (a) show a relation between the cavity power and the linewidth of the Lamb dip.

The width of the NICE-OHMS signal is measured with respect to the intra-cavity power. See figure 19 (b). The measurements are fitted with a power broadening profile. It can be observed that the measured values lie close to the fitted line thus proportional to the increase of intra-cavity power. The linewidth (FWHM) of the Lamb dip is proportional to the width of the NICE-OHMS phase signal. Since the induced phase shift from NICE-OHMS is relatively steep, and surrounded by a Doppler broadened profile, the measured width will be rather less compared to the linewidth of the Lamb dip. However the uncertainty in the measured width of the NICE-OHMS signals is smaller compared to the measured linewidth of the Lamb dip.

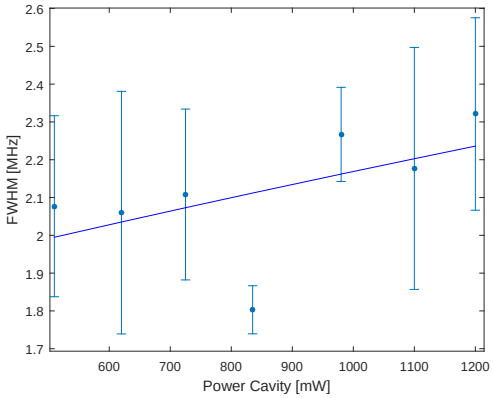

(a) The linewidth (FWHM) of the Lamb dip as a function of the intra-cavity power P_c measured in mW. The measurements are fitted with power broadening profile. The fitted results $\Gamma_0 = 1.796 \pm 0.122$ MHz and $P_s = 2182$ mW.

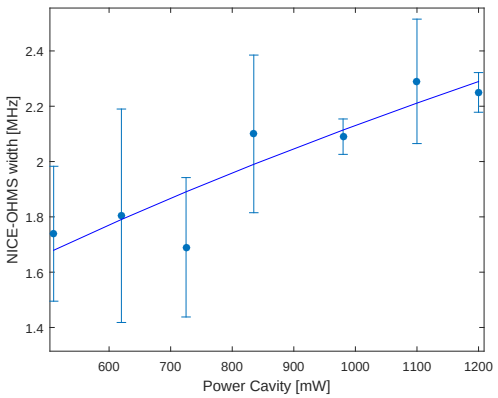

(b) The width of the NICE-OHMS signal as a function of the cavity power is measured. The measurements are fitted with power broadening profile. Fitted results, $\Gamma_0 = 1.015 \pm 0.064$ MHz, $P_s = 293.6$ mW.

Figure 19: Measurements of the width of the NICE-OHMS phase signal and linewidth (FWHM) of the saturated absorption peak, as a function of the intra-cavity power measured in mW. The error bars are plotted for each measurement.

The transit time broadening was calculated to be $\Delta\nu_{transit} = 48.45$ kHz. This means that the transit time broadening differs by a factor of 35 of the measured linewidth of the Lamb dip. The transit time broadening also affects less in fitted result for the width of the NICE-OHMS signal by a factor of 20. At higher optical powers the beam waist can be expanded in order to reduce transit time broadening.

A relative comparison can be made with the work from Jan Hald [8]. They've reached a linewidth of $\Gamma = 470$ kHz at pressure 0.90 Pa and optical power 30 mW. If we neglect the fitted results from the linewidth of the Lamb dip, since the uncertainty is larger. Instead compare Jan Hald's results to our measured results from NICE-OHMS width. Our results differ by a factor of 2 compared to Jan Hald's fitted results. The fitted linewidth is measured to be $\Gamma_0 = 1.015 \pm 0.064$ MHz. The pressure broadening linewidth can be calculated as, $\Gamma_p = a \cdot P$, where a is the pressure broadening coefficient and P the pressure. The pressure broadening coefficient is given by $a = 234$ kHz/Pa [8]. The pressure broadening linewidth is calculated to be $\Gamma_p = 257.4$ kHz. The value for pressure equal to $P = 1.1$ Pa which is believed to be the pressure of the acetylene cell. The natural linewidth for small saturation

power is given by, $\Gamma_0 = \Gamma_{transit} + a \cdot P$ [8]. This do not agree with the exact measured linewidth for zero optical power. For our measured linewidth the pressure will be around $P \sim 4$ Pa. The results show that the pressure of the acetylene cell is relatively higher than predicted. The pressure broadening is significantly larger and constitute a large amount to the measured linewidth.

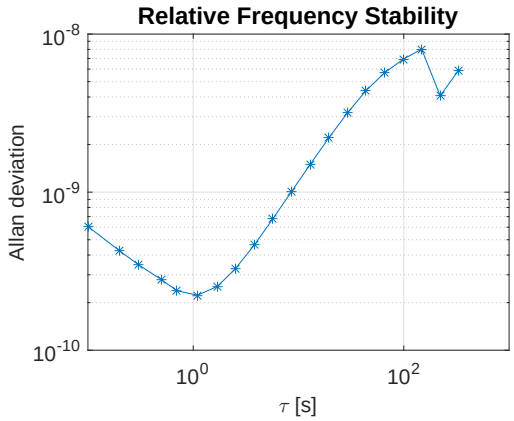

Figure 20: Allan deviation plotted for data in 100 second measurements of the laser frequency difference. The NICE-OHMS phase signal is generated as an error signal under lock. The beating of the two signals are measured within a integration time.

The Allan deviation shows the average frequency deviation over different time scales. The Allan variance is given by,

$$\sigma_y^2 = \frac{1}{2}\langle(\overline{y_2} - \overline{y_1})^2\rangle \tag{27}$$

where $\overline{y_i}$ is the mean of the measured frequency deviation over a integration time τ,

$$\overline{y_i} = \frac{1}{\tau}\int_t^{t_i+\tau} y(t)dt \tag{28}$$

The Allan deviation is determined by the frequency difference with respect to a second laser source in a given measured time τ. See figure 20. The second laser source is a NKT BasiK X15. A NICE-OHMS signal is generated as an error signal under lock. The beating of the signals are measured with another oscilloscope, Rohde & Schwarz RTO1044. The Allan deviation was measured at short integration times. The Allan deviation is close to $2.22 \cdot 10^{-10}$ near 10 seconds. The Allan deviation for integration times above 10 seconds increases. This can be compared to the work from Jan Hald. The average fraction frequency instability reaches $6 \cdot 10^{-14}$ at an integrating time of 150 s [8]. This may be related to the piezo electric element, which tripped off for larger integration times. This made it difficult to measure the beat frequency, therefore data with short integration times were collected. The temperature of the second laser source was varied in order to tune the wavelength. The second laser source was rather sensitive to temperature variations. The frequency of the stabilized laser depends on pressure of the acetylene cell, temperature and optical power.

A lock-in amplifier was used in this project for an increase in signal-to-noise ratio (SNR). The measured SNR values for the second harmonic frequency lock-in signal were relatively higher compared to the first harmonic frequency for both methods used in this project. The NICE-OHMS signal for 40 mW laser power was measured to be SNR = 3.35. When modulating the cavity length, the obtained lock-in signal of the second harmonic frequency was not as predicted. The second derivative of the intensity line shape is more asymmetric. The collected lock-in signal for the second harmonic frequency is identical with the first harmonic frequency. The amplitude of the signal decreases for higher harmonics which also can be observed from the signals. See Appendix B.

6 Conclusion

A successful saturation absorption spectroscopy was made on molecular acetylene $^{13}C_2H_2$ based on the ro-vibrational transition P(16):$\nu_1 + \nu_3$. The saturated absorption line shapes were analyzed and a linewidth of $\Gamma_0 = 1.796 \pm 0.122$ MHz for zero optical power was found. The uncertainty of the Lamb dip signals were larger compared to the width of the NICE-OHMS signal. This may be related to more noise in Lamb dip signal. A low-pass filter could be connected to the wire right before the oscilloscope. The width from the NICE-OHMS signal was measured and a linewidth of $\Gamma_0 = 1.015 \pm 0.064$ Mhz for zero optical power was found. This linewidth is assumed to be the natural linewidth. The linewidth of the Lamb dip is supposedly the pressure broadened linewidth. The pressure broadening was found to be significantly larger than the transit time broadening by a factor of 20. From the Allan deviation a relative frequency stability of $2.22 \cdot 10^{-10}$ at an integration time of 10 seconds was measured. The relative frequency stability in our project was measured to be much lower compared to work of Jan Hald. This is presumably caused by the variations in piezo response, sound noise in the laboratory when collecting data and temperature variations on the second laser source. The frequency of the laser can experience small drifts which can be further improved in the future.

References

[1] Fritz Riehle. Frequency Standards Addison Wesley, Massachusetts, 2nd edition, 1994.

[2] Recommended values of standard frequencies for applications including the practical realization of the metre and secondary reppresentations of the second, CIPM, October 2007.

[3] Laser Physics Peter W. Milonni, Joseph H. Eberly, 2010

[4] Atomic Physics, C.J Foot, 2004

[5] An Iodine Based Thermal Optical Frequency Reference using NICE-OHMS Detection, Sigrid Skovbo Adsersen, June 2016

[6] Doctoral Thesis, Further development of NICE-OHMS, Patrick Ehlers, Umeå University, 2014

[7] Wikipedia Voigt profile, `https://en.wikipedia.org/wiki/Voigt_profile`,

[8] Fiber laser optical frequency standard at 1.54 μm, Jan Hald, Lars Nielsen, Jan C. Petersen, Poul Varming and Jens E. Pedersen2 2011

[9] Cavity Enhanced Spectroscopy on Ultra cold Atoms, Martin Romme Henriksen, August 2014

A

Experimental setup for LOCK-IN Amplifier

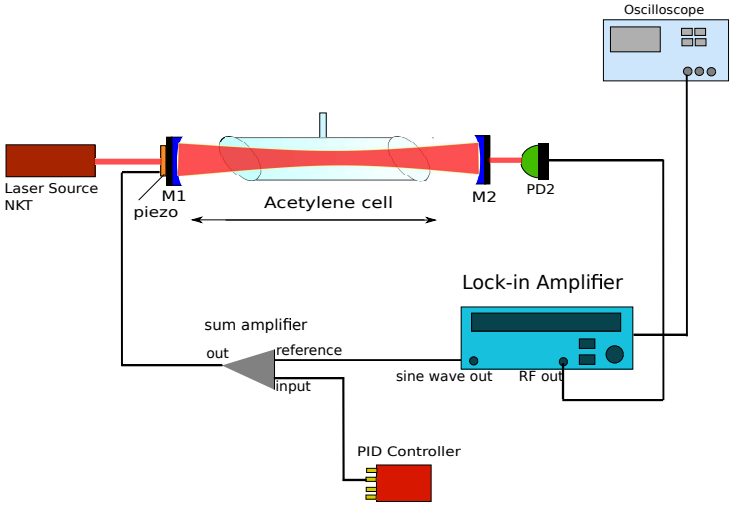

Figure 21: The experimental setup for the lock-in amplifier. The signal from the cavity is detected by the photo detector and is further applied to the lock-in amplifier which is connected to the oscilloscope. The reference sine wave signal from the lock-in samplifier is fed into a sum-amplifier. The PID-controller is also connected to the sum-amplifier. The output of the sum-amplifier is fed into the piezo on the cavity mirror.

B

The collected lock-in signals

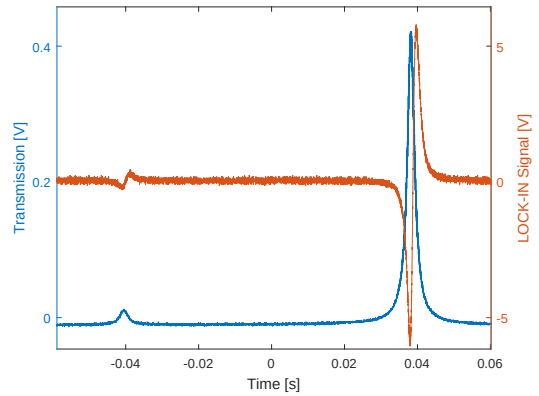

(a) Transmission and first harmonic frequency signal

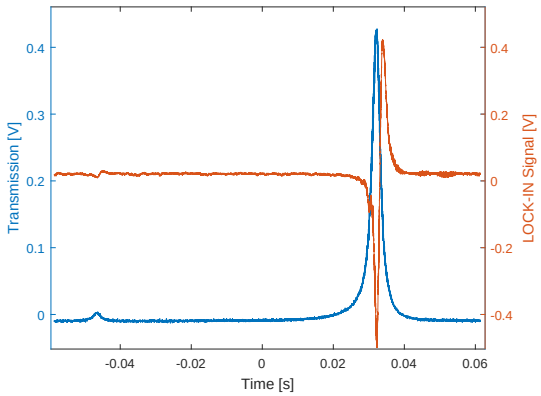

(b) Transmission and second harmonic frequency signal.

Figure 22: Collected data of transmission signal along with lock-in signals for both first and second harmonic frequency. The signals are with respect to cavity piezo position given in time. The cavity length is modulated.

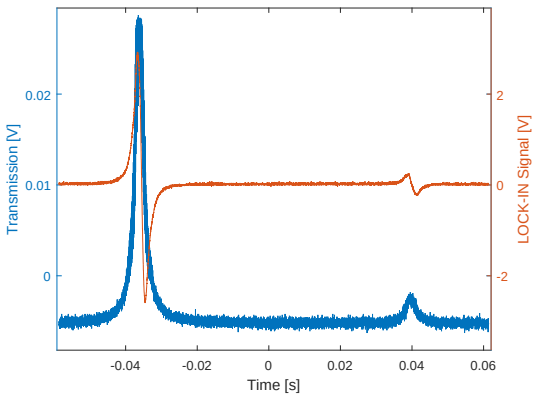

(a) Transmission and first harmonic frequency signal

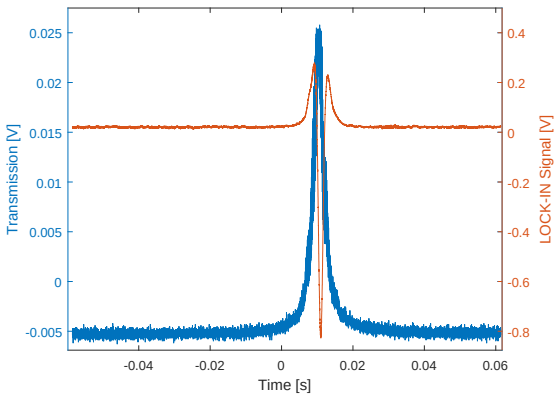

(b) Transmission and second harmonic frequency signal

Figure 23: Collected data of transmission signal along with lock-in signals for both first and second harmonic frequency. The signals are with respect to cavity piezo position given in time. The frequency of the laser is modulated.